Three-dimensional lithospheric structure below the New Zealand Southern Alps

Monica D. Kohler
Department of Earth and Space Sciences, University of California, Los Angeles, California, USA

Donna Eberhart-Phillips
Institute of Geological and Nuclear Sciences, Dunedin, New Zealand

Received 27 August 2001; revised 9 November 2001; accepted 14 November 2001; published 11 October 2002.

[1] Uppermost mantle seismic structure below the Southern Alps in South Island, New Zealand, is investigated by teleseismic *P* wave travel time residual inversion. The three-dimensional tomographic images show a near-vertical, high-velocity (2–4%) structure in the uppermost mantle that directly underlies thickened crust along the NNE-SSW axis of the Southern Alps. The center of the high-velocity anomaly lies to the east of the Alpine fault which bounds Pacific and Australian plate rocks. The oblique collision of these plates resulted in the uplift of the Southern Alps during the past 5–7 m.y. Also, a high-velocity anomaly (3–5%) corresponding to the Hikurangi subduction zone lies to the northeast of the Southern Alps anomaly, and low-velocity anomalies (−3%) underlying parts of northwestern and southern South Island may be signatures of late Tertiary extension and volcanism. The data consist of teleseismic arrival times from the New Zealand National Seismograph Network and arrival times recorded during the 1995–1996 Southern Alps Passive Seismic Experiment. Crustal heterogeneity was accounted for by back projecting the rays through an independently obtained three-dimensional crustal velocity and Moho depth model. The Southern Alps uppermost mantle velocity anomalies are most simply explained by lithospheric thickening below the center of convergence accompanied by thinning and asthenospheric upwelling adjacent to the region of convergence. *INDEX TERMS:* 8102 Tectonophysics: Continental contractional orogenic belts; 8120 Tectonophysics: Dynamics of lithosphere and mantle—general; 7218 Seismology: Lithosphere and upper mantle; 8180 Tectonophysics: Evolution of the Earth: Tomography; *KEYWORDS:* Lithosphere, Southern Alps, uppermost mantle, *P* wave velocity

Citation: Kohler, M. D., and D. Eberhart-Phillips, Three-dimensional lithospheric structure below the New Zealand Southern Alps, *J. Geophys. Res.*, *107*(B10), 2225, doi:10.1029/2001JB000182, 2002.

1. Introduction

[2] The Southern Alps in South Island, New Zealand, are the product of oblique continental collision between the Pacific and Australian plates (Figure 1). The central segment of the ~800-km-long, NNE-SSW trending Alpine fault bounds Pacific plate rocks to the east which are moving south and also overthrusting Australian plate rocks, resulting in the uplift of the Southern Alps during the past 5–7 m.y. [*Wellman*, 1953; *Walcott*, 1978; *Kamp et al.*, 1989; *Norris et al.*, 1990]. Because the Southern Alps are a young (<10 m.y. old), active orogeny, the underlying lithospheric seismic structures provide valuable clues about the dynamic relationships among mountain uplift, lithospheric deformation, and associated uppermost mantle flow. South Island, and the Southern Alps in particular, has been the target of several recent seismic experiments. Here we present the results of three-dimensional (3-D) tomographic imaging of the lithosphere below the Southern Alps using the multinetwork data. The images exhibit a 200-km-deep, 100-km-wide, subvertical high-velocity anomaly in the uppermost mantle that directly underlies thickened crust in the convergent region.

[3] The Pacific and Australian plates are converging obliquely in South Island, and lithospheric thickening is taking place to accommodate the shortening [*Walcott*, 1998]. The convergence in northern South Island is accommodated by a broad region of faulting in the overlying Australian plate and northwest subduction of the Pacific plate at the Hikurangi Trench. By contrast, in southwestern South Island the Australian plate is oceanic and is subducting eastward below the Pacific plate at the Puysegar Trench and Fiordland Trough. Convergence of the continental blocks between the subduction zones in central South Island has resulted in >3 km of uplift in central South Island where the Southern Alps are currently uplifting 5–10 mm/yr [*Wellman*, 1979; *Bull and Cooper*, 1986; *Kamp et al.*, 1989]. The Marlborough and Fiordland regions are where the transitions from subduction to continental collision take place (Figures 1 and 2).

0148-0227/02/2001JB000182$09.00

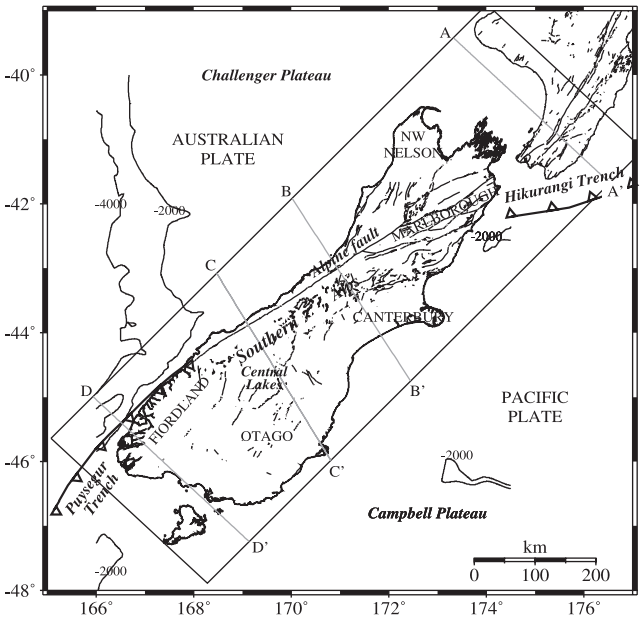

Figure 1. South Island, New Zealand plate boundary tectonic setting. The box outlines the solution space for which *P* wave seismic velocity heterogeneity is obtained. The shaded lines mark locations of *P* wave heterogeneity cross sections. Southernmost North Island is shown in the northeast corner. Bathymetry contours for −2000 and −4000 m are shown.

[4] The Alpine fault crosses most of South Island and accommodates 50–70% of total plate motion [*Cooper and Norris*, 1994; *Sutherland and Norris*, 1995; *Beavan et al.*, 1999; *Sutherland et al.*, 2000]. Total relative plate motion is 39–46 mm/yr, equivalent to 37–40 mm/yr of right-lateral strike-slip motion parallel to the fault and 11–22 mm/yr of convergent motion normal to the fault in central South Island near the Southern Alps [*Walcott*, 1979, 1998; *DeMets et al.*, 1990, 1994; *Norris et al.*, 1990; *Cooper and Norris*, 1994]. The onset of convergence is thought to have resulted directly from the changing position of the Australian–Pacific instantaneous pole of rotation [*Molnar et al.*, 1975; *Walcott*, 1978, 1998]. Displacement has become increasingly oblique over the last 10 m.y. [*Molnar et al.*, 1975; *Walcott*, 1979, 1998; *Smith*, 1981; *Allis*, 1986; *Sutherland*, 1995]. An instantaneous pole jump to the WSW 5–6 m.y. ago introduced a small component of convergence on the Alpine fault initiating Southern Alps uplift [*Sutherland*, 1995; *Walcott*, 1998]. The Alpine fault has undergone 150–175 km of dextral slip and 70–110 km of shortening since 5–7 m.y. ago [*Walcott*, 1979, 1998].

[5] The plate boundary crosses South Island continental crust as a broad zone of distributed deformation. The width of deformation is narrower (∼100 km) to the north and increases to ∼200 km in Otago defined by finite shear strain measurements calculated from geodetic retriangulation [*Walcott*, 1978, 1998; *Norris et al.*, 1990] and *SKS* splitting measurements [*Klosko et al.*, 1999]. Seismicity is distributed in a region 100–300 km wide, mostly east of the Alpine fault [*Walcott*, 1978; *Leitner et al.*, 2001]. The broad zone supports the hypothesis that deformation below the Australian-Pacific plate boundary includes pervasive, widespread ductile deformation rather than simple faulting through the lithosphere [*Molnar et al.*, 1999]. However, aseismic subduction of mantle lithosphere below and detached from the thickened crust cannot be ruled out [e.g., *Waschbusch et al.*, 1998]. Surface crustal deformation is asymmetric across the plate boundary, with most occurring near and east of the Alpine fault [*Norris et al.*, 1990]. The upper mantle below South Island is found to be highly anisotropic from *SKS* splitting measurements [*Klosko et al.*, 1999]. Fast directions in most of northern and central South Island are approximately parallel to the Alpine fault and axis of the Southern Alps (i.e., the plate boundary), and the average splitting time is 1.6 s [*Klosko et al.*, 1999]. The fast polarization directions provide evidence for simple shear distributed over a wide region that is accommodating the oblique plate motion [*Molnar et al.*, 1999].

[6] Crustal thickness varies from 30 to 45 km across the Southern Alps [*Woodward*, 1979; *Allis*, 1986; *Smith et al.*, 1995; *Wilson and Eberhart-Phillips*, 1998]. The crust thickens asymmetrically from west to east with the deepest portion offset 10 km east of the highest topography [*Davey et al.*, 1998]. The Southern Alps are thought to be underlain by a lower crust ductile detachment zone along which material above the detachment travels obliquely up the fault and out of the deforming region [*Wellman*, 1979; *Koons*, 1990; *Norris et al.*, 1990]. Thickened crust due to the development of a root is wider and thickest at the southern end south of the highest peaks and terminates abruptly at the northern end [*Reilly and Whiteford*, 1979; *Norris et al.*, 1990].

[7] The tomographic study presented here was motivated by previous results which showed a kinematic relationship between thickened crust and high velocities in the upper mantle below the actively deforming transpressional Pacific–North America plate boundary in southern California [*Kohler*, 1999]. Those results suggested mechanical and/or thermal coupling between thickened lower crust and upper mantle below the Transverse Ranges mountain belt on the plate boundary. *Kohler and Davis* [1997] and *Kohler* [1999] obtained high-resolution tomographic images from temporary and permanent network teleseismic data that suggested that the entire lithosphere below the compressional zone had thickened in a narrow, vertical sheet. Imaging of *P* wave travel time residuals showed that the high-velocity upper mantle anomaly comprises a 60- to 80-km-wide sheet of mantle material similar to that found in earlier studies [*Raikes*, 1980; *Humphreys and Clayton*, 1990] but, in addition, showed that it occurred directly below an 8- to 10-km-deep crustal root. They found evidence that deformation in the ductile lower crust and mantle lithosphere may be partially coupled mechanically and thermally if the thickening is occurring together in response to ongoing convergence. *Houseman et al.* [2000] further showed that the geometry of the Transverse Ranges high-velocity anomaly could be predicted by theoretical dynamical experiments in which the mantle lithosphere was modeled as a cold, dense downwelling driven by gravitational instability and external plate convergence.

[8] Previous studies have given some insights into deep lithospheric structure in several South Island locations.

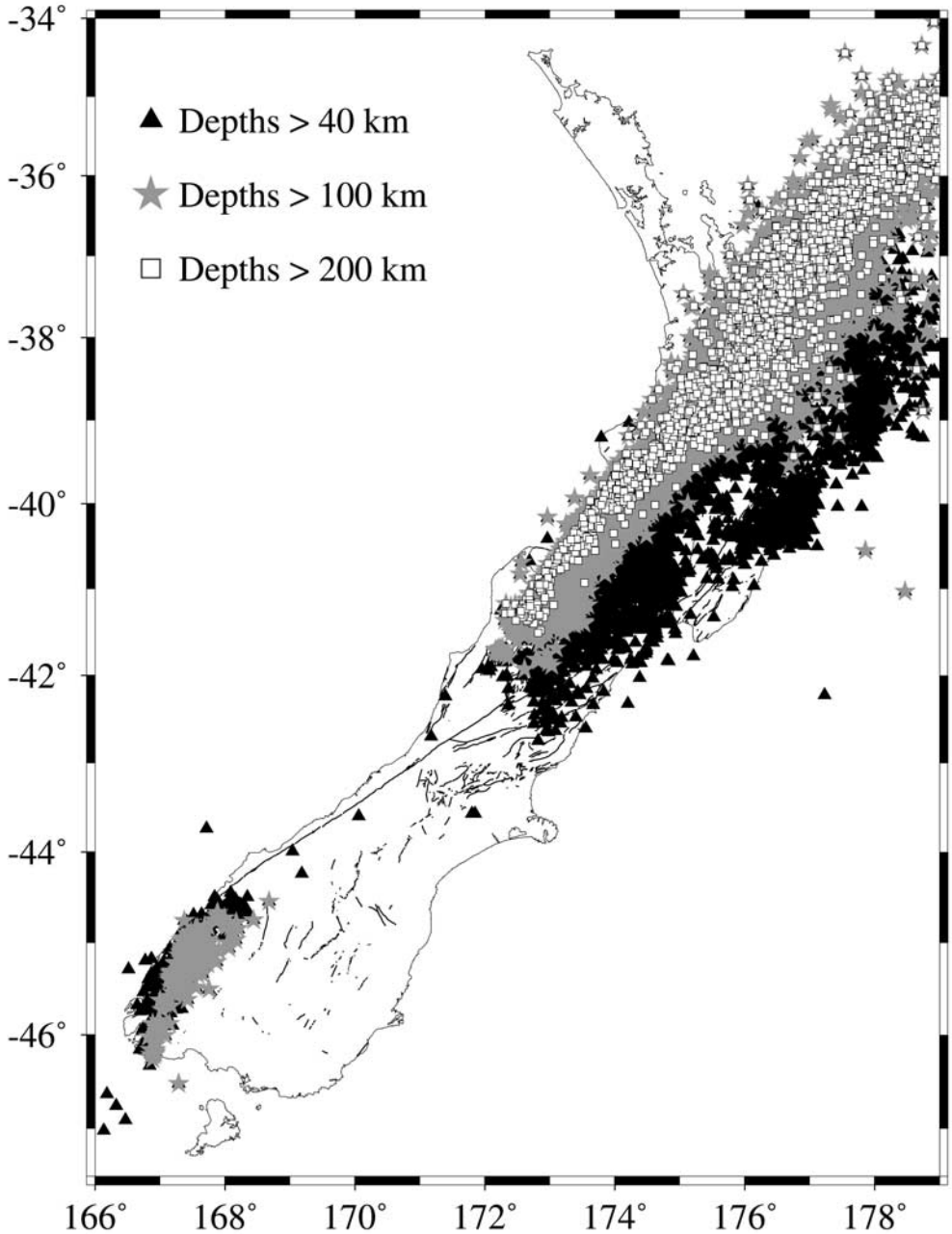

Figure 2. Locations of earthquakes deeper than 40 km recorded by the New Zealand National Seismic Network between January 1990 and August 1998.

Stern et al. [2000] inferred a high-velocity body in central South Island extending to 150 km in depth from a 2-D seismic profile using forward modeling with a varied Moho but uniform crustal velocity. Using local earthquake data, *Eberhart-Phillips and Reyners* [2001] image a high-velocity body in Fiordland below 80 km in depth in the mantle of the Pacific plate which appears to restrain subduction and to cause the Australian subducted slab to bend to vertical. In northern South Island, seismicity shows a sharp along-strike edge to the subducted slab [*Anderson and Webb*, 1994]. By obtaining a deep 3-D image of the whole South Island we can determine how these features are related. In this study, we use teleseismic tomography to understand the transition from subduction to oblique motion on the Alpine fault and its effect on lithospheric deformation.

2. Travel Time Data

[9] We performed travel time inversions with the goal of obtaining tomographic images to understand and provide geometric constraints to the dynamics of plate boundary lithospheric deformation. Our inversion data are from several different permanent and temporary networks: the permanent short-period New Zealand National Seismograph Network, the temporary Southern Alps Passive Seismic

Experiment, and several other temporary short-period networks. The combination of data from these arrays provides good station and ray path coverage throughout the entire South Island.

[10] The New Zealand National Seismograph Network (NZNSN) has been producing digital waveform data since 1990 and makes up the majority of travel time data in our inversions. The network is composed of high-quality, uniformly instrumented short-period stations with an average spacing of ~100 km. The Wellington (WEL) network is a subset of the NZNSN and is denser to monitor subduction-related seismicity in the Wellington region. In addition, several recent experiments took place whose data have been incorporated into the NZNSN database. They include temporary seismic networks in the Marlborough and Fiordland regions. Instrumentation, digitization, and timing methods are uniform for every station of the NZNSN and temporary arrays. Travel times are determined by NZNSN operators and reported in the NZNSN waveform and seismicity catalog. Teleseismic waveforms are recorded in triggered format; therefore only waveforms from the larger earthquakes were recorded.

[11] Additional ray path coverage is provided by travel times measured from Southern Alps Passive Seismic Experiment (SAPSE) stations. The goal of SAPSE [*Stern et al.*, 1996; *Anderson et al.*, 1997] was to obtain a comprehensive view of seismicity and three-dimensional variations in lithospheric structure in order to understand how deformation in the obliquely convergent plate boundary is accommodated along the Alpine fault and within the Southern Alps. The passive experiment (November 1995 to April 1996) was run concurrently with two active transects to obtain a fully integrated seismic data set for crustal and upper mantle three-dimensional imaging. The SAPSE array consisted of 26 broadband and fourteen 1-Hz short-period, three-component stations. The stations were broadly distributed but centrally weighted toward the central Alpine fault and transect region. Although the SAPSE earthquakes were recorded primarily in the Southern Alps, several stations were collocated with NZNSN stations. We used the colocated stations to adjust the residuals by a constant time shift for each earthquake in order to make them consistent with the larger number of evenly distributed regional NZNSN residuals. The SAPSE earthquake travel times were determined by cross correlation relative to clearly recorded first-arrival *P* waveforms at reliable stations.

3. Inversion Methods

[12] The travel time inversions for velocity variations were computed using a 2-D Fourier series expansion and block parameterizations for comparison. The absolute travel time residual for the *i*th earthquake and *j*th station is

$$d_{ij}^{A} = T_{ij}^{\mathrm{ob}} - T_{ij}^{\mathrm{pred}} + \Delta T_j, \tag{1}$$

where

$$\Delta T_j = \Delta T_{\substack{\text{source}\\ \text{location}}} + \Delta T_{\substack{\text{origin}\\ \text{time}}} + \Delta T_{\substack{\text{lower}\\ \text{mantle}}} + \Delta T_{\substack{\text{crust+}\\ \text{Moho}}} + \Delta T_{\substack{\text{upper}\\ \text{mantle}}} + \Delta T_{\text{anisotropy}}, \tag{2}$$

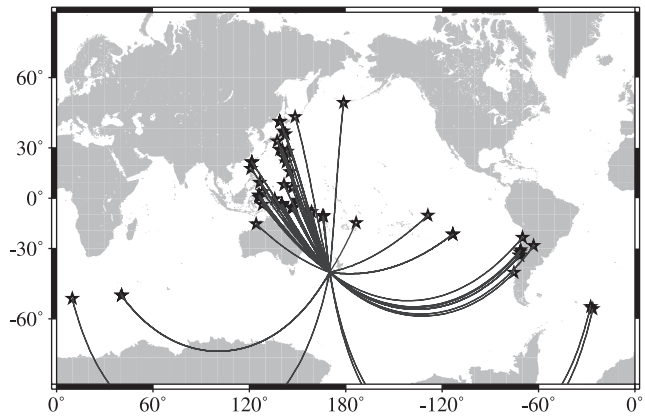

Figure 3. Earthquakes used in inversions. Great circle ray paths are shown to a central location in South Island in the Mercator projection.

and the predicted travel time is computed using the iasp91 Earth model [*Kennett and Engdahl*, 1991]. The advantage of using teleseismic rays is that $\Delta T_{\substack{\text{source}\\ \text{location}}}$, $\Delta T_{\substack{\text{origin}\\ \text{time}}}$, and $\Delta T_{\substack{\text{lower}\\ \text{mantle}}}$ are essentially identical for all teleseisms corresponding to the same earthquake recorded on South Island stations. Therefore, when we demean the travel times for an individual earthquake to compute the relative residuals, we can neglect the contributions from those terms. The relative residual is then

$$d_{ij} = d_{ij}^{A} - \frac{1}{n_j}\sum_{j=1}^{n_j} d_{ij}^{A}, \tag{3}$$

where n_j is the number of stations that recorded a particular earthquake.

[13] In order to demean the residuals we desire earthquakes with the largest, most evenly distributed residuals so that we remove a regional mean and not a localized mean. Thus we limited earthquakes to those with ≥15 arrival time picks across the entire South Island and Wellington. Most teleseisms recorded in New Zealand are from subduction zone earthquakes from the northwest and northeast (e.g., Fiji-Tonga, Aleutians, Indonesia, Japan, and Kamchatka). So we separated the remaining earthquakes into 45° back azimuth bins and 10° distance bins ($\Delta \geq 30°$) and chose one earthquake from each bin to keep ray path coverage as uniform as possible. This left us with 56 teleseismic events (Figure 3) and 831 travel time picks.

[14] We did not include anisotropy in our velocity modeling as there is no unique way to incorporate the *SKS* splitting measurements into teleseismic *P* wave travel time inversions. The fast directions observed for horizontal anisotropy are almost uniform, and the splitting times in our study area are not widely different [*Klosko et al.*, 1999]. Our *P* wave velocity variations, obtained from near-vertical ray paths, cannot be attributed to anisotropy and should be viewed as independent features that coexist with the regional anisotropy.

[15] Rays are back projected from each station through initially flat-layered Earth structure, and travel times are expressed as the path integral of a function of velocity and

distance traveled through each depth interval in the parameter space. The travel time for the ith ray is

$$T_i = \int_{S_i} \frac{ds}{V(\vec{r})}. \tag{4}$$

Using Fermat's principle to obtain the travel time with respect to the starting model V_0,

$$T_i = \int_{S_i^0} \frac{ds}{V_0(\vec{r})}. \tag{5}$$

The travel time residual is then

$$\delta T_i = T_i - T_i^0 \cong -\int_{S_i^0} \frac{\delta V_p(\vec{r})}{V_0(\vec{r})^2} ds = \sum_L^{\#\text{layers}} -\left(\frac{D \cdot \delta V_p(\vec{r})}{V_0(\vec{r})^2}\right)_L, \tag{6}$$

where velocity perturbation $\delta V = V - V_0$ and distance traveled

$$D = \int_{S_0} ds. \tag{7}$$

The rays in subsequent iterations were ray traced through updated three-dimensional structure using a horizontal interface between 0.1 km depth intervals.

[16] Expanding δV_p in 2-D Fourier series,

$$\delta T_i = \sum_L^{\#\text{layers}} -\left\{\left[\frac{D}{V_0(\vec{r})^2}\right]\left[\sum_{m=0}^{m_{\max}}\sum_{n=0}^{n_{\max}} \lambda_{mn}\left(a_{mn}\cos\frac{\pi m x}{l}\cos\frac{\pi n y}{h} + b_{mn}\sin\frac{\pi m x}{l}\cos\frac{\pi n y}{h} + c_{mn}\cos\frac{\pi m x}{l}\sin\frac{\pi n y}{h} + d_{mn}\sin\frac{\pi m x}{l}\sin\frac{\pi n y}{h}\right)\right]\right\}_L \tag{8}$$

where λ_{mn} are normalization constants, a_{mn}, b_{mn}, c_{mn}, and d_{mn} are the expansion coefficients for which we solve, and $-l/2 \le x \le l/2$ and $-h/2 \le y \le h/2$ define the dimensions of the solution space. The short dimension l is 660 km, and the long dimension h is 1320 km. The corresponding Fourier expansion indices are $m_{\max} = 3$ and $n_{\max} = 6$. Depth parameterization consists of 10 layers, each 40 km thick. The diagonal pivoting method was used to factor the resulting normal matrix in order to obtain the solution to the real system of linear equations iteratively (LAPACK subroutine package) [*Anderson et al.*, 1999]. Five iterations were enough to ensure that the solution had converged with a significant variance reduction. Initial residual values varied between −2.2 and 2.5 s after crustal correction. The total variance reduction after five iterations was 42%, corresponding to an average travel time residual fit of 0.3 s. The test for singularity was made by estimating the condition number of a matrix by comparing the Gaussian elimination pivots to exact zero; the normal matrix never came close to singularity. Resolution tests shown in section 4 for the 2-D Fourier approach illustrate how the final images should be interpreted in light of data coverage.

[17] We imaged the lithosphere using grid parameterization as well and found both approaches to be satisfactory for this application. The solution space was divided into 50 × 50 km and 75 × 75 km blocks for comparison with the global basis function results. The conjugate gradient method for least squares problems was used to solve the large, sparse system of equations (LSQR method) [*Paige and Saunders*, 1982]. The Fourier expansion does a good job of imaging low-frequency velocities where the data are sparse and relatively homogeneous. It does not produce artifacts where there is ray path coverage, and it produces only very low amplitude, low-frequency oscillation at the edges of the solution space. The grid parameterization (at about the same minimum wavelength) is faster but only assigns velocity to blocks with ray path coverage. The grid approach produces a small amount of low-amplitude artificial structure at the edges of the solution space as well. Its drawback is that it does not image low-frequency structure well when we want to examine small features using smaller blocks. We present our results in the 2-D Fourier format and compare them with the 75 × 75 km grid results to show that except for small-wavelength details, the smoothed images are essentially the same.

[18] The 3-D crustal V_p and V_p/V_s structure for most of South Island has been obtained by inverting arrival times from several hundred local earthquakes recorded by permanent and temporary seismometer networks [*Eberhart-Phillips and Reyners*, 1997, 2001; D. Eberhart-Phillips and S. Bannister, Three-dimensional crustal structure in the Southern Alps region of New Zealand from inversion of local earthquake and active source data, submitted to *Journal of Geophysical Research*, 2001, hereinafter referred to as Eberhart-Phillips and Bannister, submitted manuscript, 2001]. We used this model of crustal velocity heterogeneity and Moho depth variations to remove their effects on the teleseismic travel times. We ray traced the teleseismic rays through the 3-D crustal model to 60 km in depth, calculated the travel times for each ray, and subtracted them from the total travel time through the solution space. The local earthquake 3-D velocity images show strong lateral variations in the entire crust with strong correlations between anomalies and tectonic structures such as subducting slabs, terranes, and seismicity. Higher velocities reflect the subducting Pacific plate in the Hikurangi subduction zone in northern South Island. The pattern of velocity heterogeneity in the upper crust is broadly consistent with mapped geology, and velocities range from ~4.5 to 7.2 km/s.

4. Resolution Tests

[19] Ray path coverage is not uniform, and we expect better resolution where the ray paths are denser. In anticipation of checkerboard resolution tests we computed the geographical locations for the segments of all ray paths that lie between the depth interval boundaries corresponding to the final solution. The resulting ray path segments are shown in Figure 4, and they distinguish regions where ray path coverage is uniform and dense from regions where it is sparse.

[20] In order to assess the resolution of our images at different wavelengths we performed a number of traditional checkerboard resolution tests using different synthetic Earth structures. The input synthetic Earth structures are defined by a unique, limited combination of Fourier coefficients whose maximum amplitudes are assigned 3%. We deter-

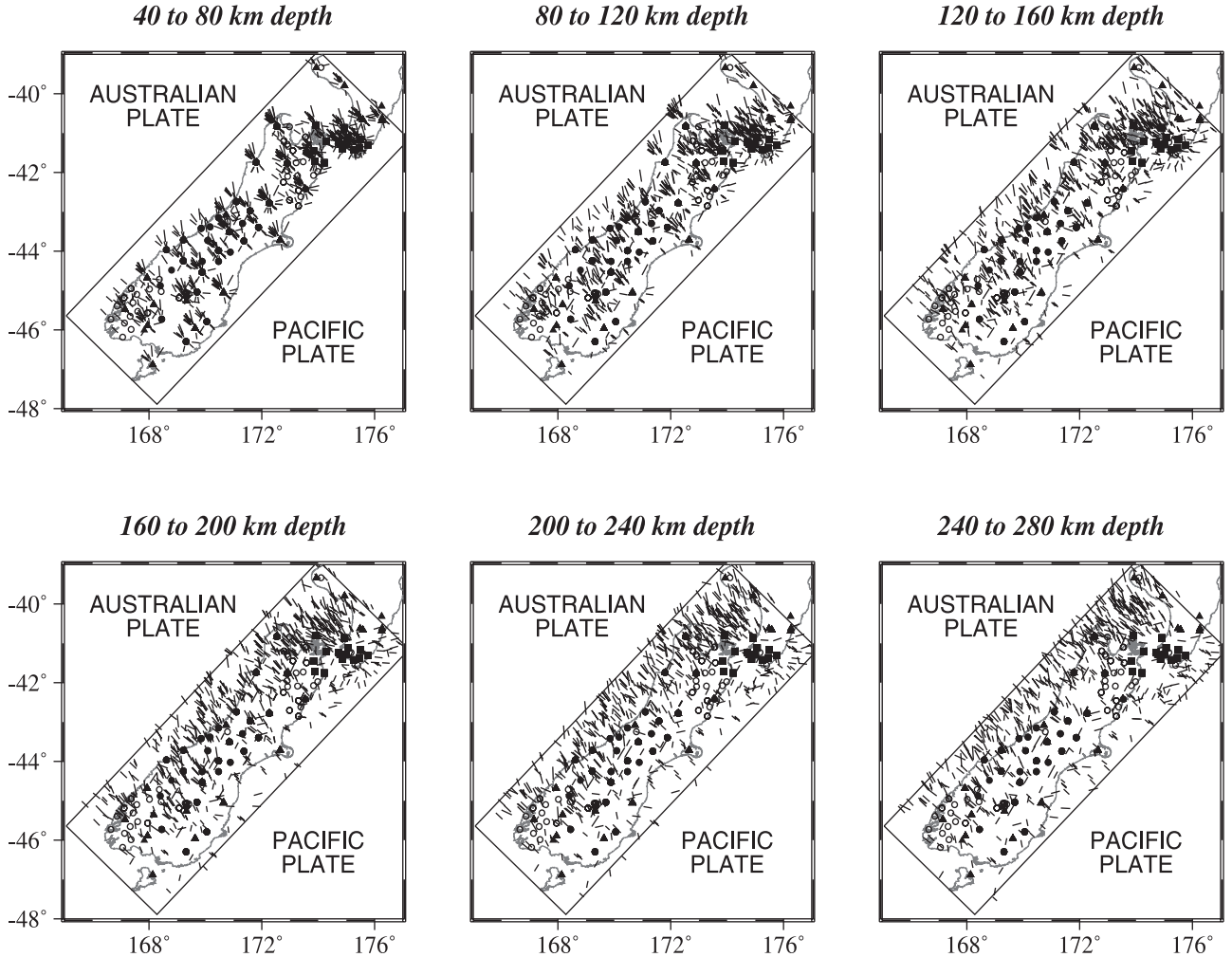

Figure 4. Ray path segments for depth intervals whose velocity structures correspond to the starting model and to those shown in Figures 5, 7, and 9.

mined resolution by inverting synthetic travel time residuals resulting from forward modeling through the various synthetic Earth structures. The inversions use the same inversion parameters (e.g., number of data and earthquakes, damping, number of iterations) as the real data inversions and illustrate where amplitude may be diminished or structure geometries distorted.

[21] For the first test, initial Earth structure was defined by the $m = 2$, $n = 4$ Fourier terms with amplitudes $a_{mn} = b_{mn} = c_{mn} = 0$ and d_{mn} assigned so that input structure varied between −3% and +3% at all depths. Rays were projected through the synthetic Earth models, and the resulting synthetic travel time residuals were inverted for Earth structure. Initial patterns and results are shown in Figure 5 for depths of 60, 100, 140, 180, 220, and 260 km. Recovered synthetic Earth structure has a similar pattern to the input pattern for most of the solution space. We believe this is due to our windowing of the data to minimize the number of regions predominantly sampled by a large number of rays within a limited back azimuth or distance range. Recovery grows poorer for deeper layers and for regions northeast and southeast of the array. The pattern of recovered structure follows the ray path distribution geometry. Recovered structure shows that the bias in paths from the northwest tends to elongate structures in that direction. At depths >220 km, structure becomes smeared horizontally because of thinner ray path coverage that is radiating away from the stations. Maximum recovered velocity amplitude is 40% relative to the initial Earth structure for depths <100 km and decreases for greater depths, reaching a minimum of 20% at the bottom of the solution space.

[22] The second set of resolution inversions was performed to test how anomalies at depth were smearing along ray path directions, in particular to the northwest. The synthetic input models consisted of vertical, single-column anomalies at points along four cross sections (Figure 6, left). Each column is 110 km in diameter and extends from 40 to 400 km in depth. The input structures were digitized at each depth interval and expressed as 2-D Fourier series in order to calculate the spectral power of the recovered structure. Fourier amplitudes were normalized so that the input structure varied between −3% and +3% at all depths. Cross sections of the recovered structure for each region (Figure 6, right) indicate the degree of elongation and smearing that has occurred. The northwest elongation is most significant where ray path coverage is heavy and biased toward the

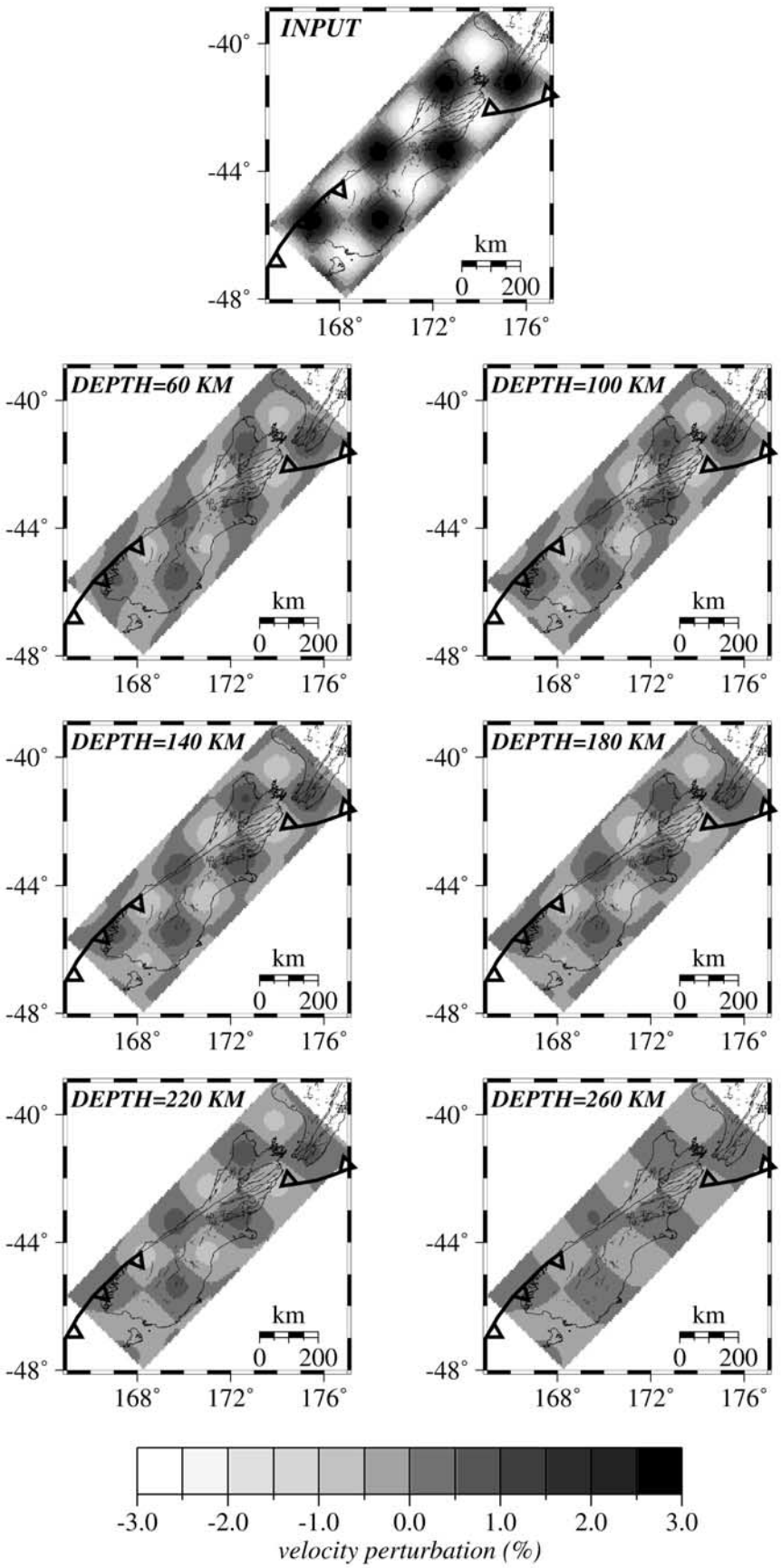

Figure 5. (top) Input and (bottom) resulting patterns from checkerboard resolution test for depths of 60, 100, 140, 180, 220, and 260 km.

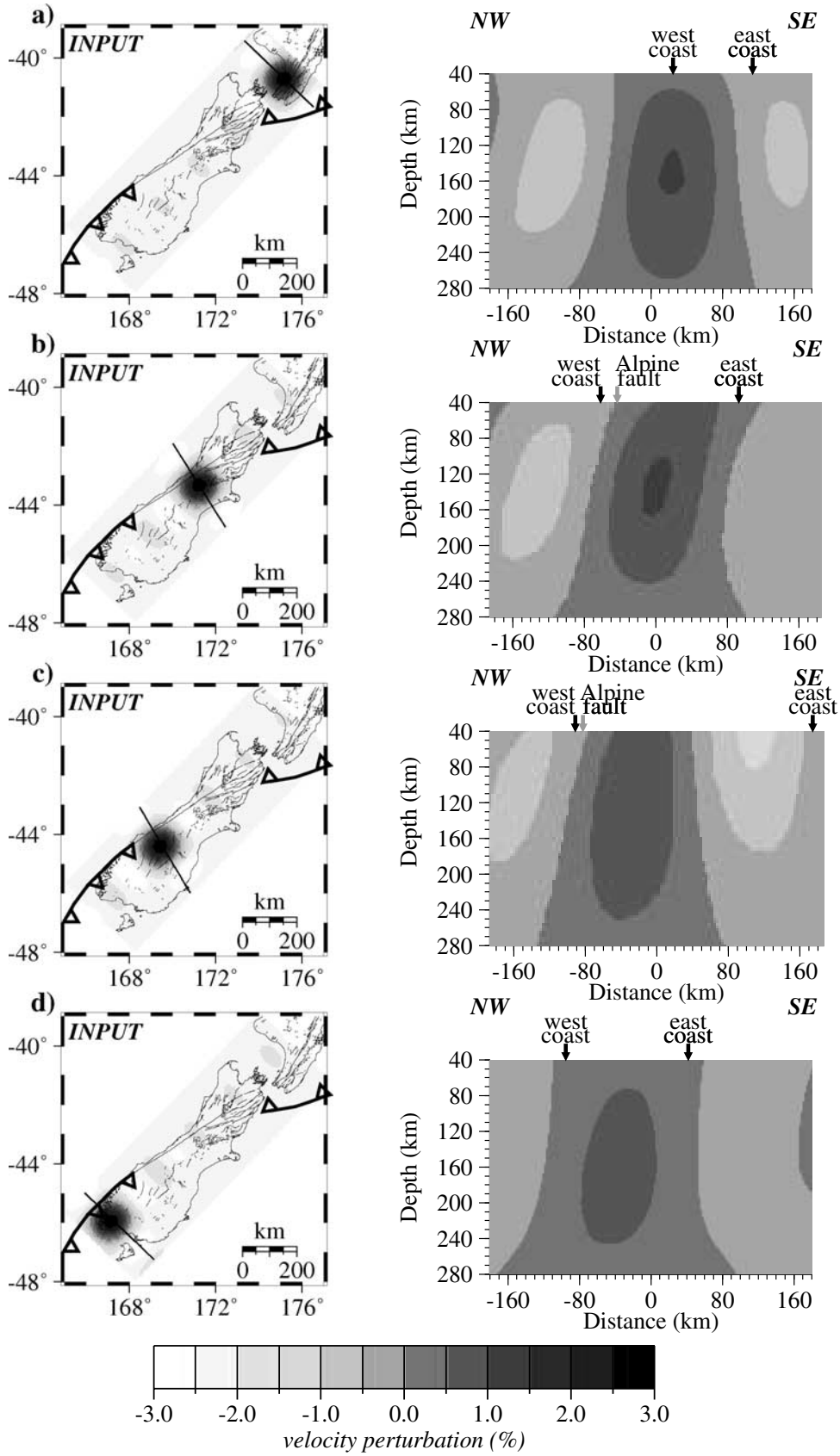

Figure 6. (left) Input and (right) resulting patterns from vertical column resolution tests along cross sections (a) A-A', (b) B-B', (c) C-C', and (d) D-D' shown by heavy solid line in plan view. Cross-section locations are the same as those shown in Figure 1. Intersections with the west and east coastlines are shown by solid arrows, and Alpine fault location is shown by shaded arrow.

northwest (e.g., B-B'). Spreading to both the northwest and southeast occurs where ray path coverage is less dense and therefore less biased in one direction (e.g., D-D') and when coverage is more distant from the stations (e.g., at the bottom of all cross sections). The resolution inversion also tends to decrease the magnitude of the anomaly at greater depths.

5. Results

[23] Tomographic images resulting from the teleseismic travel time inversions are shown in Figures 7 and 8. The solution space corresponding to significant ray path coverage is outlined by the rectangular bounding box whose long (NNE-SSW) dimension was made roughly parallel to the axis of the Southern Alps in order to examine approximately perpendicular cross sections below the convergent zone. The velocity perturbation values were held constant within each layer and linearly interpolated for different depths in the final images.

[24] Map views of the three-dimensional *P* wave velocity variations are shown in Figure 7, and the scale at the bottom shows where the perturbation in percent is different from zero. Velocities are mapped at the midpoint of each depth interval. The first image for the depth of 60 km (Figure 7) is the Fourier expansion of perturbations in the top mantle layer. In the 60-km-depth view the highest velocities correspond to the Pacific plate in the Hikurangi subduction zone, and there is some northerly smearing of high velocity as expected from the resolution tests (Figure 5). Velocity perturbations reach a maximum of 3%, and the location correlates strongly with slab-related seismicity (Figure 2). A long swath of high-velocity perturbations (up to 2%) occurs below the Southern Alps, stretching from the Hikurangi subduction zone to the Puysegar subduction zone. The width of the anomaly varies from 60 to 100 km. Low velocities (−3%) occur along the entire stretch of the easternmost Australian plate and in the Otago and Canterbury volcanic regions on the east coast. At 100 km in depth the Hikurangi slab continues to be the highest-velocity feature, and it is now apparent that the Southern Alps high-velocity anomaly is a near-vertical or steeply west dipping feature. It continues to follow the Southern Alps uplift, which is distributed throughout a broad region east of the fault. The center of the high-velocity anomaly lies east of the Alpine fault and is more highly correlated with the highest topography than it is with the Alpine fault.

[25] At 140 km in depth the slab orientation has changed, but the Southern Alps anomaly is similar to shallower lithosphere. Note that the apparent change in slab orientation occurs because the slab is near vertical below 100 km in depth in Northwest Nelson, while it is moderately dipping in the North Island (Figure 2), and thus the low-velocity anomaly underlying Taranaki is in the overlying mantle (Figure 7, red triangle in southern North Island). By 180 km depth the Southern Alps anomaly has begun to fade away or has moved northwest, and low-velocity (−1.5%) patches now occur in central South Island, most notably in the Central Lakes region. The slab signature is still strong, with slab orientation becoming more NE-SW with depth. At 220 km the Southern Alps anomaly is gone or has a northwestern tail, and the offshore influence of slab structure is still apparent in the high velocities occurring along the northwest coast. These features continue to the bottom of the solution space where ray path coverage eventually becomes too sparse to resolve structure geometry.

[26] Four cross sections perpendicular to the axis of the Southern Alps are shown in Figure 8. Earthquakes deeper than 40 km that have occurred within 20 km of the cross section are plotted on each depth slice. The cross sections are in order northeast to southwest with locations marked by the shaded lines in Figure 1. The intersections with the western and eastern coastlines are shown by solid arrows, and the location of the Alpine fault is shown by the shaded arrow. The first cross section (A-A') shows the high velocities and seismicity associated with the subducting slab in the Hikurangi subduction zone. The second and third cross sections (B-B' and C-C') exhibit a near-vertical, high-velocity uppermost mantle anomaly beneath the thickened portion of the Southern Alps, with little or no associated seismicity. The fourth cross section (D-D') is less straightforward as it shows structures more closely related to the Southern Alps anomaly than to the shallow Puysegar subduction zone, in which the Australian plate is subducting nearly vertically beneath the Pacific plate.

[27] The results of the resolution tests validate the observation that the upper mantle high-velocity anomaly is a coherent, large-scale structure but also indicate that a higher velocity (+4%) may be realistic for the Southern Alps feature imaged as +2%. Similarly, 5% may be realistic for the Hikurangi slab imaged as 3%. The resolution tests also support the lateral location and width of the large-scale anomalies for depths less than ~220 km in the final images.

[28] The inversions were also performed with grid parameterization as described in section 3, and the results of the 75 × 75 km grid dimensions are shown in Figure 9 to emphasize the similarities between the continuous basis functions and interpolated grid values. The variance reduction is similar, and thus the results are complementary for interpreting uncertainty in the shape of velocity anomalies. The velocities shown in Figure 9 were computed by linearly interpolating the velocity values found for the center of each grid. The depth intervals are the same as before. Figure 9 exhibits the same high-velocity structures below the Hikurangi subduction zone and Southern Alps and low velocities adjacent to the convergent regions. However, as resolution becomes weaker at 180 km in depth, the grid image is patchy with more peripheral artifacts. The similarities support the use of 2-D Fourier expansions as an alternative to representing seismic velocity structure in which spatially variable spectral information can be obtained directly from the solution, and the results can be automatically smoothed in regions where there are little or no data.

6. Discussion

[29] One of the most pronounced features in the tomographic results at all depths in Figure 7 is the high-velocity body beneath northern South Island and southern North Island produced by the Hikurangi subduction zone. Its location and geometry change with depth in such a way that it appears to rotate counterclockwise, consistent with seismicity patterns (Figure 2). Subduction zone seismicity shows that the subducting plate is moderately dipping

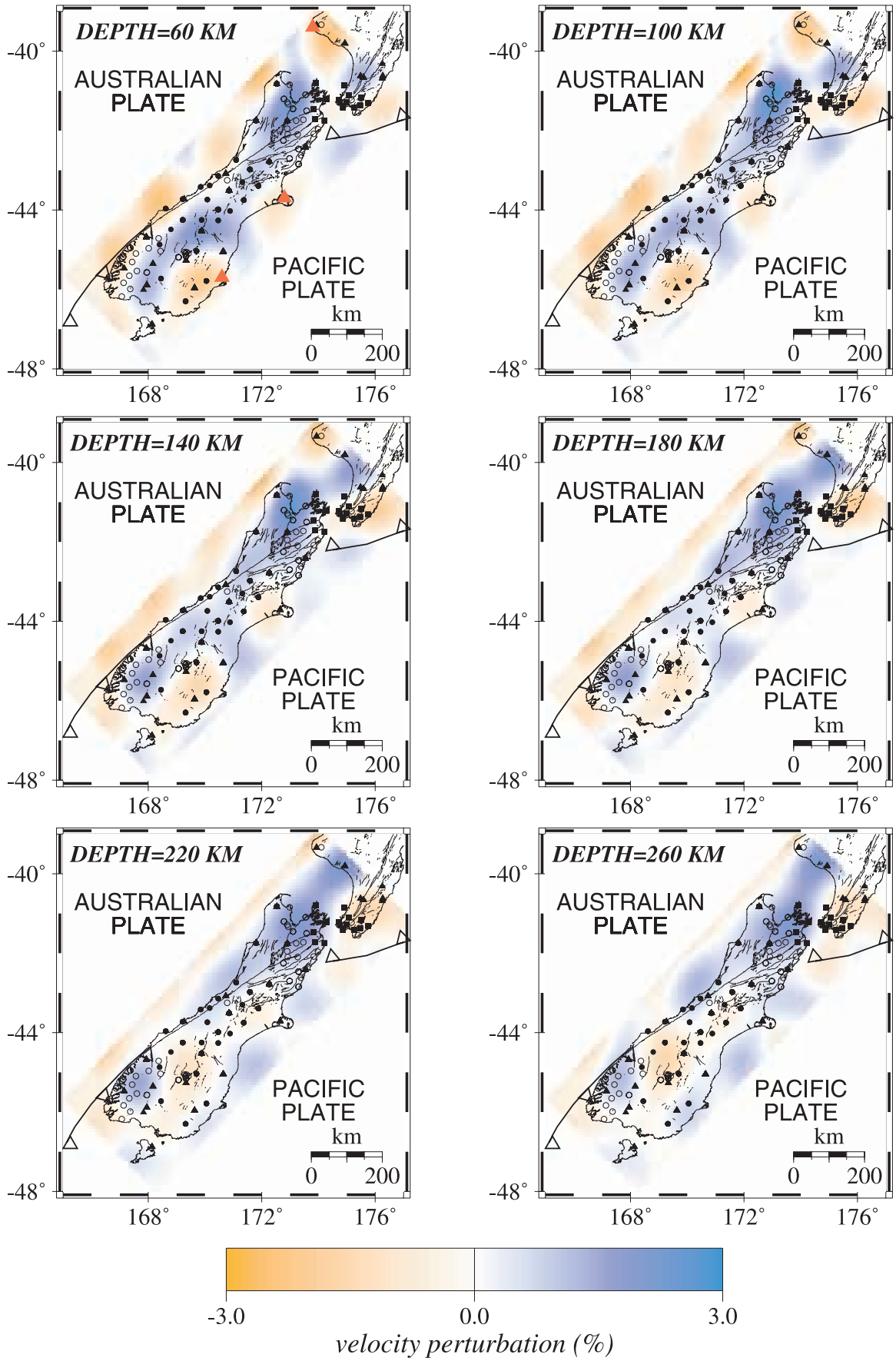
DEPTH=60 KM
DEPTH=100 KM
DEPTH=140 KM
DEPTH=180 KM
DEPTH=220 KM
DEPTH=260 KM
AUSTRALIAN PLATE
PACIFIC PLATE
km
0
200
-40°
-44°
-48°
168°
172°
176°
-3.0
0.0
3.0
velocity perturbation (%)

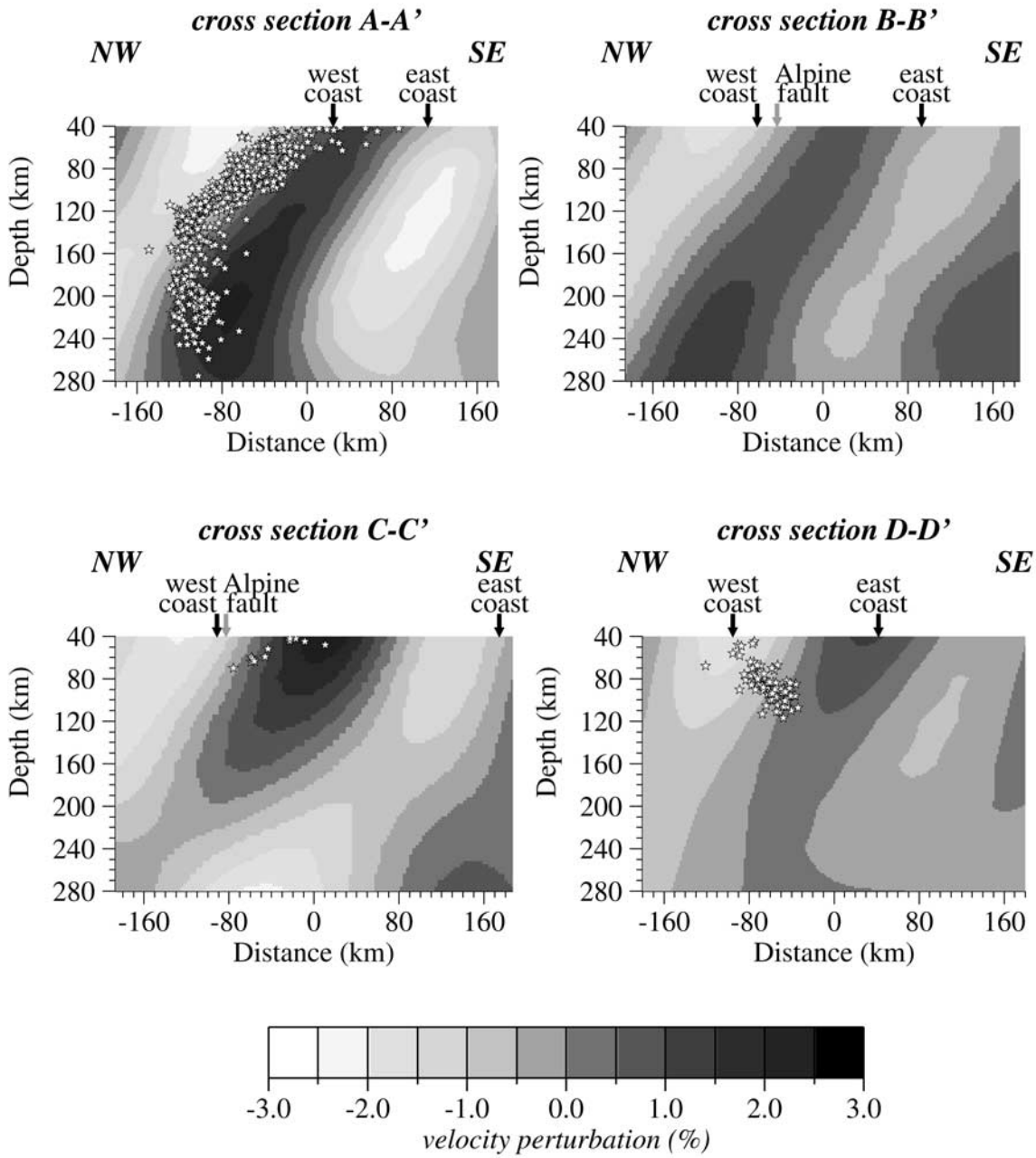

Figure 8. *P* wave velocity variations in four cross sections approximately perpendicular to the axis of the Southern Alps in order northeast to southwest. Locations of the cross sections are shown in Figure 1. Stars show hypocenters of earthquakes located within 20 km of cross section. Intersections with the west and east coastlines are shown by solid arrows, and Alpine fault location is shown by shaded arrow.

below North Island where active subduction is taking place and that it becomes vertical below Northwest Nelson [*Eberhart-Phillips and Reyners*, 1997]. The plate interface gradually becomes permanently locked in the Marlborough region and the already subducted slab rotates along with overlying faults [*Walcott*, 1998; *Eberhart-Phillips and Reyners*, 1997]. Lithospheric cross section A-A' shows that much of the seismicity occurs on the top (northwest) face of the slab (Figure 8). Seismicity studies also show that there are occasional deep earthquakes to 350 km in depth under Northwest

Figure 7. (opposite) *P* wave velocity variations beneath South Island for depths of 60, 100, 140, 180, 220, and 260 km. Symbols show locations of stations corresponding to Southern Alps Passive Seismic Experiment (SAPSE) (solid circles), New Zealand National Seismograph Network (NZNSN) (triangles), Wellington Network (WEL) (squares), and other temporary networks (open circles) which provided travel time data. Red triangles show regions that have experienced volcanism <10 m.y. ago.

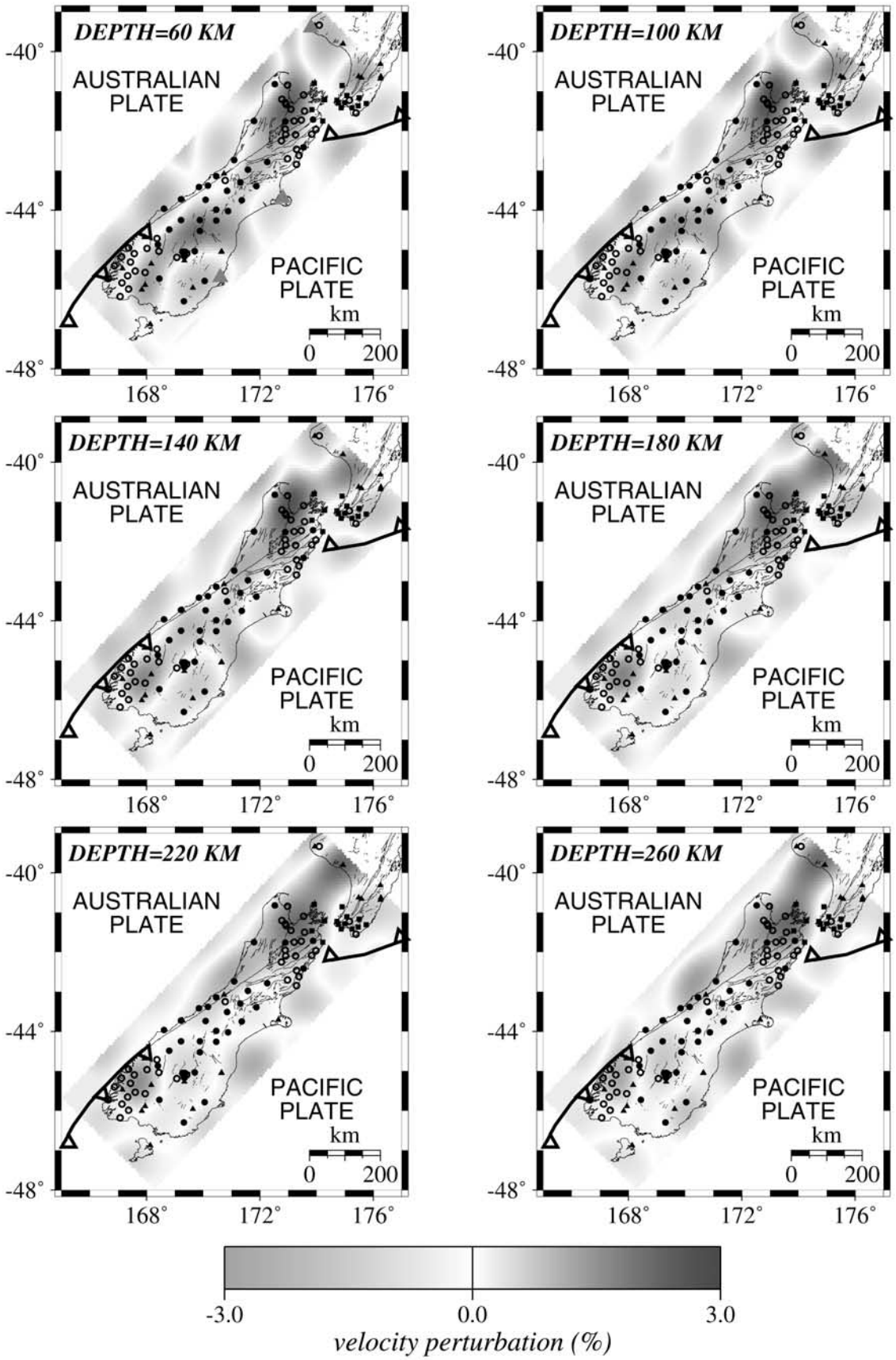

Figure 9. *P* wave velocity variations beneath South Island for depths of 60, 100, 140, 180, 220, and 260 km using grid parameterization.

Nelson [*Anderson and Webb*, 1994; *Downes*, 1994] consistent with the depth extent of the slab in Figure 8. Global 3-D tomography [*Bijwaard et al.*, 1998; *Engdahl et al.*, 2000] shows a generally similar Hikurangi slab, although coarser in resolution and weaker in amplitude, indicating that our results are not affected by velocity heterogeneity outside the region.

[30] The tomographic images (Figure 7) show that the transition from northwest subducting slab to the relatively high velocities below the Southern Alps is gradual on these length scales. The Southern Alps high-velocity anomaly between Marlborough and Fiordland extends to less than ~180-km depth in contrast to the deep Hikurangi subduction zone. The Southern Alps anomaly does not change orientation with depth like the slab, and its geometry can be visualized as a long sheet descending into the mantle. Note that the shapes of the high-velocity features in B-B' and C-C' are partly due to smearing along ray paths. Since the island (and station distribution) is narrowest at that section, there is little crossfire of ray paths on the northwest, and thus the high-velocity may be smeared along ray paths from the northwest. This means that a shallower high-velocity feature that had a larger velocity perturbation could equivalently fit these data.

[31] High velocities extend from the 100-km-thick slab in Northwest Nelson to southern South Island suggesting a gradual change from a slab environment associated with deep seismicity in the oceanic lithosphere to continental lithospheric collision conditions which are characterized by a lack of deep seismicity. The images suggest that continental mantle lithospheric deformation takes over where subduction stops, but they do not provide evidence for a sharp oceanic lithospheric slab edge where the deep seismicity ends. These features are all present and continuous in the grid parameterization results (Figure 9).

[32] The Southern Alps high-velocity anomaly directly underlies thickened crust almost everywhere within South Island. Crustal thickness is estimated from the isovelocity surface corresponding to 7.8 km/s determined from local earthquake travel time inversions [*Eberhart-Phillips and Reyners*, 1997, 2001; Eberhart-Phillips and Bannister, submitted manuscript, 2001] and is shown in Figure 10. Figure 10 also shows subduction-related variations in the lower crust of the overlying plate. Crustal thickness values are consistent with active source profiles [e.g., *Van Avendonk et al.*, 1999] and receiver function analysis [*Parker*, 1999]. The deepest Moho in central South Island corresponds to the axis of the Southern Alps, and the crustal root broadens as the plate boundary region deformation also broadens in Otago (Figure 10). The Southern Alps crustal root is asymmetric with a sharper gradient on the western side [*Davey et al.*, 1998]. The spatial correlation between thickened crust and upper mantle high velocities has also been observed in travel time residuals from three teleseismic earthquakes recorded on two dense seismic profiles across the Southern Alps [*Stern et al.*, 2000]. A handful of small mantle earthquakes up to 73 km deep have been recorded in central South Island beneath the Southern Alps with good depth constraints [*Reyners*, 1987]. They correspond to the faster (and presumably colder) portion of the Southern Alps high-velocity anomaly shown in Figure 7 (60 km in depth).

[33] The Fiordland high-velocity structure at 100 km in depth is continuous with the Southern Alps high-velocity anomaly (Figure 7). This feature has also been imaged with local earthquakes [*Eberhart-Phillips and Reyners*, 2001] as a high-velocity body in the Pacific mantle abutting the subducted Australian plate. The Fiordland feature is deeper than the Southern Alps feature. It extends to at least 220 km in depth (Figure 7), where a low-velocity region separates it from Hikurangi slab high velocities. Neither the teleseismic nor local earthquake studies of Fiordland find high velocities associated with the subducted Australian plate (Figure 8, cross section D-D'). It is relatively young (20–40 m.y. old) and may be thinner, warmer, and less dense than older slabs.

[34] Consistently low velocities occur along the entire coast west of the Alpine fault and are clearly evident in the large, late residuals recorded at west coast stations. Whereas continental lithosphere below South Island is probably thickened by >100 km, lithospheric thickness outside the convergent region may be less. The simplest explanation for the relatively low velocities within the Australian plate is that the lithosphere is thinner and that the deeper ray segments may be sampling asthenosphere. The velocity is particularly low (less than −2% at 60 km in depth) southeast of the Challenger Plateau on the Australian plate where there is a major change from oceanic to continental lithosphere [*Sutherland et al.*, 2000].

[35] The low-velocity patches in eastern Otago and Canterbury are in agreement with wide-angle reflection-refraction seismic observations that have been associated with the Dunedin volcano [*Godfrey et al.*, 2000]. Godfrey et al. found low velocities indicative of hot fluids in a highly reflective region of the lower crust. The locations coincide with surface regions that experienced volcanism ~6 m.y. ago (Canterbury) and ~10 m.y. ago (eastern Otago) and that exhibit high heat flow today (Figure 7, red triangles in 60-km-depth plot). There is also low velocity in the western North Island underlying Mount Taranaki which has been built by volcanism during the last 5 m.y. (Figure 7, red triangle in southern North Island in 60-km plot). The low velocities below 200 km in depth in the Central Lakes region are consistent with horizontal flow of the asthenosphere around the high-velocity subducted lithospheric slabs [*Koons et al.*, 1999].

[36] The Southern Alps tomographic high-velocity anomaly is evidence for plate boundary deformation that occurs in a broad, diffuse zone [e.g., *Molnar et al.*, 1999]. Although the majority of plate motion takes place on the Alpine fault, seismicity is diffuse throughout central South Island. The Alpine fault forms the northwestern boundary between the region of diffuse seismicity that extends 70 km to the southeast and the region of very little seismicity to the northwest [*Eberhart-Phillips*, 1995]. The seismicity and crustal deformation indicate that the Australian block is coherent with little internal deformation, but the southern Pacific block shows distributed deformation on a wide range of strike-slip and thrust faults [*Leitner et al.*, 2001]. The Pacific block is internally weak as suggested by short-wavelength gravity anomalies whose source has been interpreted as highly mobile graywacke crust that lacks the ability to transmit shear stresses [*Eberhart-Phillips*, 1995; *Stern*, 1995]. If convergence is symmetric about the plate boundary, the geometry of the anomaly and crustal thicken-

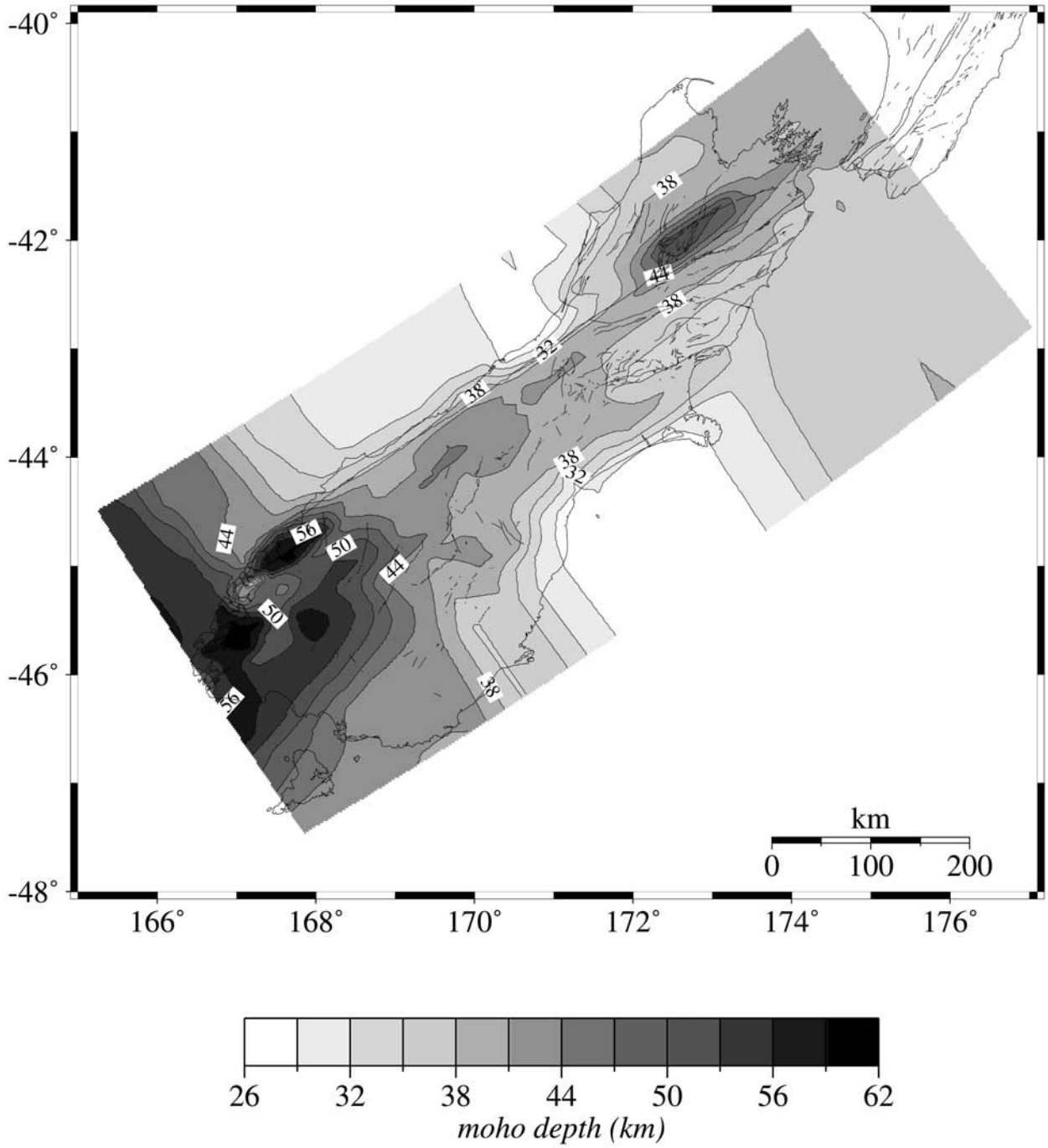

Figure 10. Crustal thickness variations inferred from the isovelocity curve corresponding to 7.8 km/s. Velocity contour data are from Eberhart-Phillips and Bannister (submitted manuscript, 2001).

ing suggests that the center of convergence is parallel to the Southern Alps axis but at a distance of 50–70 km southeast of the Alpine fault. If the deformation is more like delamination [e.g., *Wellman*, 1979], the anomaly may correspond to asymmetric, northwestward downwelling of mantle lithosphere. M. Gerbault and F. Davey (3-D lateral crustal thickening in continental oblique collision: An example from the Southern Alps, New Zealand, submitted to *Geophysical Journal International*, 2002) applied oblique boundary conditions to numerical block models of the Australian and Pacific plates with varied rheology and obtained a crustal root and lithospheric thickening of the Pacific plate along an axis 10°–20° from the plate boundary. Downwelling of cool, dense Pacific mantle centered southeast of the Alpine fault supports their model.

[37] The usefulness of obtaining 3-D seismic images is further underscored while trying to understand the effects of shear in conjunction with convergence on lithospheric deformation. Dextral shear occurs along the Alpine fault, and shear wave splitting fast polarization measurements

parallel to the plate boundary illustrate how simple shear constitutes one factor controlling lithospheric deformation [*Molnar et al.*, 1999]. Large vertical shear may be another factor if the cold, denser uppermost mantle is deforming in a downwelling manner. By means of geodynamic numerical experiments, *Houseman et al.* [2000] found that a vertical downwelling due to gravitational instability and external convergence explained the presence of high-velocity anomalies below a young, actively deforming orogeny. This mode of deformation has been invoked to explain the mantle seismic structures below South Island [*Molnar et al.*, 1999; *Stern et al.*, 2000]. Large shear strains are predicted to develop in the thickened, dense lithosphere as it descends into the asthenosphere [*Houseman and Molnar*, 1997; *Houseman et al.*, 2000]. The combination of large shear strains and relatively cold lithosphere with a depressed, brittle-plastic transition zone characterizes the South Island continental collisional environment in which subcrustal earthquakes are occurring. The 3-D images can be used to constrain future 3-D numerical geodynamic models that combine subduction and downwelling below South Island.

7. Conclusions

[38] Teleseismic *P* wave travel time inversions using data from a number of permanent and temporary seismic networks were performed in order to obtain seismic tomographic images of lithosphere below the Australian-Pacific plate boundary in South Island, New Zealand. The imaging focuses on the Hikurangi and Puysegur subduction zones, the continental lithospheric collision region in central South Island, and regions within the broad zone of plate boundary deformation. The Hikurangi subduction zone is imaged as a deep, high-velocity feature whose location corresponds to the descending slab. Most of the deep seismicity occurs on the top face of the imaged slab, whose dip becomes increasingly vertical with depth. The depth extent of the imaged slab corresponds to the deepest seismicity.

[39] A long, steeply west dipping sheet of high velocities (2–4%) occurs below the entire stretch of the Southern Alps, and its location correlates highly with thickened crust. The Southern Alps high-velocity anomaly varies from 60 to 100 km in width, where the narrowest portion corresponds to the narrowest region of crustal deformation in central and northern South Island, and the widest portion corresponds to the wider plate boundary deformation zone in Otago. The spatial correlation between uppermost mantle high velocities and crustal thickness suggests thermal and mechanical coupling between the crust and mantle at the plate boundary. The shape and seismic properties of the lithospheric anomaly are consistent with downwelling in the collision zone that is driven by relatively high densities and horizontal convergence that has produced the thickened crust and mantle lithosphere.

[40] **Acknowledgments.** This work was supported by NSF grant EAR-9805224 and the New Zealand Foundation for Research Science and Technology. Special thanks go to Tom McEvilly and Helen Anderson for envisioning and carrying out the Southern Alps Passive Seismic Experiment (NSF EAR-9418530) and the IRIS Data Management Center for providing data and technical support. We appreciate discussions with Peter Koons, Rupert Sutherland, Peter Molnar, and Paul Davis. The comments of two anonymous reviewers were especially helpful in strengthening the resolution discussion. This is Institute of Geological and Nuclear Sciences contribution 2213.

References

Allis, R. G., Mode of crustal shortening adjacent to the Alpine fault, New Zealand, *Tectonics*, *5*, 15–32, 1986.

Anderson, E., et al., *LAPACK Users' Guide*, 3rd ed., Soc. for Ind. and Appl. Math., Philadelphia, Pa., 1999.

Anderson, H., and T. Webb, New Zealand seismicity: Patterns revealed by the upgraded National Seismograph Network, *N. Z. J. Geol. Geophys.*, *37*, 477–493, 1994.

Anderson, H., D. Eberhart-Phillips, T. McEvilly, F. Wu, and R. Uhrhammer, Southern Alps passive seismic experiment, *Sci. Rep. 97/21*, Inst. of Geol. and Nucl. Sci., Lower Hutt, New Zealand, 1997.

Beavan, J., et al., Crustal deformation during 1994–1998 due to oblique continental collision in the central Southern Alps, New Zealand, and implications for seismic potential of the Alpine fault, *J. Geophys. Res.*, *104*, 25,233–25,255, 1999.

Bijwaard, H., W. Spakman, and E. R. Engdahl, Closing the gap between regional and global travel time tomography, *J. Geophys. Res.*, *103*, 30,055–30,078, 1998.

Bull, W. B., and A. F. Cooper, Uplifted marine terraces along the Alpine fault, New Zealand, *Science*, *234*, 1225–1228, 1986.

Cooper, A. F., and R. J. Norris, Anatomy, structural evolution, and slip rate of a plate-boundary thrust: The Alpine fault at Gaunt Creek, Westland, New Zealand, *Geol. Soc. Am. Bull.*, *106*, 627–633, 1994.

Davey, F. J., et al., Preliminary results from a geophysical study across a modern, continent-continent collisional plate boundary: The Southern Alps, New Zealand, *Tectonophysics*, *288*, 221–235, 1998.

DeMets, C., R. G. Gordon, D. F. Argus, and S. Stein, Current plate motions, *Geophys. J. Int.*, *101*, 425–478, 1990.

DeMets, C., R. G. Gordon, D. F. Argus, and S. Stein, Effect of recent revisions to the geomagnetic reversal timescale on estimates of current plate motions, *Geophys. Res. Lett.*, *21*, 2191–2194, 1994.

Downes, G., Exceptionally deep earthquakes in the northern South Island, *N. Z. J. Geol. Geophys.*, *37*, 127–130, 1994.

Eberhart-Phillips, D., Examination of seismicity in the central Alpine fault region, South Island, New Zealand, *N. Z. J. Geol. Geophys.*, *38*, 571–578, 1995.

Eberhart-Phillips, D., and M. Reyners, Continental subduction and three-dimensional crustal structure: The northern South Island, New Zealand, *J. Geophys. Res.*, *102*, 11,843–11,861, 1997.

Eberhart-Phillips, D., and M. Reyners, A complex, young subduction zone imaged by 3-D seismic velocity, Fiordland, New Zealand, *Geophys. J. Int.*, *146*, 731–746, 2001.

Engdahl, E. R., S. H. Kirby, and A. Villasenor, New results of a global investigation of slab morphology and seismicity using arc-centric projections of reprocessed hypocenters with a high-resolution tomographic model, *Eos Trans. AGU*, *81*(47), Fall Meet. Suppl., F1080, 2000.

Godfrey, N. J., F. Davey, and T. A. Stern, Crustal structure and thermal anomalies of the Dunedin region, South Island, New Zealand, *Eos Trans. AGU*, *81*(47), Fall Meet. Suppl., F1220, 2000.

Houseman, G. A., and P. Molnar, Gravitational (Rayleigh-Taylor) instability of a layer with non-linear viscosity and convective thinning of continental lithosphere, *Geophys. J. Int.*, *128*, 125–150, 1997.

Houseman, G. A., E. A. Neil, and M. D. Kohler, Lithospheric instability beneath the Transverse Ranges of California, *J. Geophys. Res.*, *105*, 16,237–16,250, 2000.

Humphreys, E. D., and R. W. Clayton, Tomographic image of the southern California mantle, *J. Geophys. Res.*, *97*, 19,725–19,746, 1990.

Kamp, P. J. J., P. F. Green, and S. H. White, Fission track analysis reveals character of collisional tectonics in New Zealand, *Tectonics*, *8*, 169–195, 1989.

Kennett, B. L. N., and E. R. Engdahl, Travel times for global earthquake location and phase identification, *Geophys. J. Int.*, *105*, 429–465, 1991.

Klosko, E. R., F. T. Wu, H. J. Anderson, D. Eberhart-Phillips, T. V. McEvilly, E. Audoine, M. K. Savage, and K. R. Gledhill, Upper mantle anisotropy in the New Zealand region, *Geophys. Res. Lett.*, *26*, 1497–1500, 1999.

Kohler, M. D., Lithospheric deformation beneath the San Gabriel Mountains in the southern California Transverse Ranges, *J. Geophys. Res.*, *104*, 15,025–15,041, 1999.

Kohler, M. D., and P. M. Davis, Crustal thickness variations in southern California from Los Angeles Region Seismic Experiment passive phase teleseismic travel times, *Bull. Seismol. Soc. Am.*, *87*, 1330–1344, 1997.

Koons, P. O., Two-sided orogen: Collision and erosion from the sandbox to the Southern Alps, New Zealand, *Geology*, *18*, 679–682, 1990.

Koons, P. O., P. Upton, C. M. Henderson, R. L. Enlow, and C. J. Pearson, Otago versus Canterbury: Basic differences in inherited geology and applied forces, *Misc. Publ. 107A*, p. 82, Geol. Soc. of N. Z., Wellington, New Zealand, 1999.

Leitner, B., D. Eberhart-Phillips, H. Anderson, and J. N. Nabelek, A focused look at the Alpine fault, New Zealand: Seismicity, focal mechanisms, and stress inversions, *J. Geophys. Res.*, *106*, 2193–2220, 2001.

Molnar, P., T. Atwater, J. Mammerick, and S. M. Smith, Magnetic anomalies, bathymetry and the tectonic evolution of the South Pacific since the late Cretaceous, *Geophys. J. R. Astron. Soc.*, *40*, 383–420, 1975.

Molnar, P., et al., Continuous deformation versus faulting through the continental lithosphere of New Zealand, *Science*, *286*, 516–519, 1999.

Norris, R. J., P. Koons, and A. F. Cooper, The obliquely-convergent plate boundary in the South Island of New Zealand: Implications for ancient collision zones, *J. Struct. Geol.*, *12*, 715–725, 1990.

Paige, C. C., and M. A. Saunders, LSQR: An algorithm for sparse linear equations and sparse least squares, *Trans. Math. Software*, *8*, 43–71, 1982.

Parker, P. B., Genetic algorithms and their use in geophysical problems, Ph.D. thesis, 202 pp., Univ. of Calif., Berkeley, 1999.

Raikes, S. A., Regional variations in upper mantle structure beneath southern California, *Geophys. J. R. Astron. Soc.*, *63*, 187–216, 1980.

Reilly, W. I., and C. M. Whiteford, Bouguer and isostatic anomalies, South Island, in *Gravity Map of New Zealand*, Dep. of Sci. and Ind. Res., Wellington, New Zealand, 1979.

Reyners, M., Subcrustal earthquakes in the central South Island, New Zealand, and the root of the Southern Alps, *Geology*, *15*, 1168–1171, 1987.

Smith, E. G. C., Calculation of poles of instantaneous rotation from poles of finite rotation, *Geophys. J. R. Astron. Soc.*, *65*, 223–227, 1981.

Smith, E. C. G., T. A. Stern, and B. O'Brien, A seismic velocity model for the central South Island, New Zealand, *N. Z. J. Geol. Geophys.*, *38*, 565–571, 1995.

Stern, T. A., Gravity anomalies and crustal loading at and adjacent to the Alpine Fault, New Zealand, *N. Z. J. Geol. Geophys.*, *38*, 593–601, 1995.

Stern, T. A., P. E. Wannamaker, D. Eberhart-Phillips, D. Okaya, and F. J. Davey, Mountain building and active deformation studied in New Zealand, *Eos Trans. AGU*, *78*(329), 335–336, 1996.

Stern, T., P. Molnar, D. Okaya, and D. Eberhart-Phillips, Teleseismic *P* wave delays and modes of shortening the mantle lithosphere beneath South Island, New Zealand, *J. Geophys. Res.*, *105*, 21,615–21,631, 2000.

Sutherland, R., The Australian-Pacific boundary and Cenozoic plate motions in the SW Pacific: Some constraints from Geosat data, *Tectonics*, *14*, 819–831, 1995.

Sutherland, R., and R. J. Norris, Late Quaternary displacement rate, paleoseismicity and geomorphic evolution of the Alpine fault: Evidence from near Hokuri Creek, south Westland, New Zealand, *N. Z. J. Geol. Geophys.*, *38*, 408–419, 1995.

Sutherland, R., F. Davey, and J. Beavan, Plate boundary deformation in South Island, New Zealand, is related to inherited lithospheric structure, *Earth Planet. Sci. Lett.*, *177*, 141–151, 2000.

Van Avendonk, H. J., W. S. Holbrook, J. K. Austin, and D. Okaya, Seismic velocity and wide-angle reflectivity structure of the Australian-Pacific plate boundary, South Island, New Zealand, *Eos Trans. AGU*, *80*(46), Fall Meet. Suppl., F1029, 1999.

Walcott, R. I., Present tectonics and Late Cenozoic evolution of New Zealand, *Geophys. J. R. Astron. Soc.*, *52*, 137–164, 1978.

Walcott, R. I., Plate motion and shear strain rates in the vicinity of the Southern Alps, in *Origin of the Southern Alps*, edited by R. I. Walcott and M. M. Cresswell, *Bull. R. Soc. N. Z.*, *18*, 5–12, 1979.

Walcott, R. I., Modes of oblique compression: Late Cenozoic tectonics of the South Island of New Zealand, *Rev. Geophys.*, *36*, 1–26, 1998.

Waschbusch, P., G. Batt, and C. Beaumont, Subduction zone retreat and recent tectonics of the South Island of New Zealand, *Tectonics*, *17*, 267–284, 1998.

Wellman, H. W., Data for the study of Recent and late Pleistocene faulting in the South Island of New Zealand, *N. Z. J. Sci. Technol., Sect. B*, *34*, 270–288, 1953.

Wellman, H. W., An uplift map for the South Island of New Zealand, and a model for uplift of the Southern Alps, in *Origin of the Southern Alps*, edited by R. I. Walcott and M. M. Cresswell, *Bull. R. Soc. N. Z.*, *18*, 13–20, 1979.

Wilson, D., and D. Eberhart-Phillips, Estimating crustal thickness in the central South Island, *Sci. Rep. 98/27*, Inst. of Geol. and Nucl. Sci., Lower Hutt, New Zealand, 1998.

Woodward, D. J., The crustal structure of the Southern Alps, New Zealand, as determined by gravity, in *Origin of the Southern Alps*, edited by R. I. Walcott and M. M. Cresswell, *Bull. R. Soc. N. Z.*, *18*, 95–98, 1979.

D. Eberhart-Phillips, Institute of Geological and Nuclear Sciences, Private Bag 1930, Dunedin, New Zealand. (D.Eberhart-Phillips@gns.cri.nz)

M. D. Kohler, Department of Earth and Space Sciences, University of California, Los Angeles, 595 Charles Young Dr. East, 3806 Geology Building, Los Angeles, CA 90095-1567, USA. (kohler@ess.ucla.edu)